Urban environment during pregnancy and childhood and white matter microstructure in preadolescence in two European birth cohorts

Anne-Claire Binter, Laura Granes, Elise Bannier, Montserrat de Castro, Sami Petricola, Serena Fossati, Martine Vrijheid, Cécile Chevrier, Hanan El Marroun, Mark Nieuwenhuijsen, Dave Saint-Amour, Henning Tiemeier, Mònica Guxens

Methods S1. Assessment of the urban environment

Sources of data for each exposure are summarized in Table S1.

We characterized population density as the number of inhabitants per square kilometer at the residential address. We defined building density as the sum of built area in buffer area of 300m. We characterized street intersection density as the number of street intersections in buffer areas of 300m. We calculated the density of bus stops and of bus lines as the meters and the number of stops of public transport lines in a buffer area of 300m. Density of bus stops and bus lines were not included in the PELAGIE cohort because information was missing for 70% of the participants. We calculated facility richness as the number of facility types in a buffer area of 300 m, divided by the maximum potential number of facility types, giving a score of 0 to 1. A higher value indicates a more availability of different facility types (Table S2). We characterized the percentage of type of land use in a buffer area of 300 m, including: "high density residential area", "low density residential area", "commercial and industrial units", and "transport" land uses. We built a land use diversity index calculated as the proportional abundance of each type of land use multiplied by the logarithm of that proportion, divided by the logarithm of the number of the different types of land use, in a buffer of 300 m, giving a score of 0 to 1. A higher value indicates a more even distribution of land between the different types of land uses (Table S3).

Equation of the land use diversity index

$$LUDI = \frac{-\sum_{i=1}^{m} (Pi * ln\ Pi)}{ln\ m}$$

Pi = proportion of the area occupied by land use type (class) i.

m = number of land use types (classes) present in the study area

LUDI = land use diversity index

We built a walkability index, as the mean of the deciles of population density, street intersection density, facility richness, and land use diversity index. It gives a score ranging from -1 to 1, with a higher score indicating a more walkable area (Frank et al. 2006).

Equation of the Walkability Index (WI)

$$WI = \frac{LUDI + FR + PD + CI}{4}$$

Range: $0 \leq WI \leq 1$

LUDI = land use diversity index

FR = Facility richness

PD = Population density

CI = Connectivity index

For the urban natural spaces indicators, we measured the surrounding greenness within a 300 m buffer around each address, using the Normalized Difference Vegetation Index (NDVI) derived from the Landsat 4–5 Thematic Mapper (TM), Landsat 7 Enhanced Thematic Mapper Plus (ETM +), and Landsat 8 Operational Land Imager (OLI)/Thermal Infrared Sensor (TIRS) with 30 m × 30 m resolution (courtesy of the U.S. Geology Survey). NDVI quantifies the difference between near-infrared (which vegetation strongly reflects) and red light (which vegetation absorbs). NDVI values range from -1 to 1, with higher numbers indicating more greenness. Negative values in the images have been reclassified to null values. Images were included if the cloud cover was less than 10 %, and at the greenest period of the year (i.e., between May and August). Furthermore, we created two indicators for residential proximity to the major urban green and blue spaces, as they cover different aspects of natural space exposure, i.e., easy access to recreational space. We calculated access to major green space (e.g., parks or countryside) and major blue spaces (e.g., sea, lakes, fish ponds, rivers, canals) from topographical maps as the straight-line distance from the home to nearest green or blue

space with an area greater than 5000 m2. We also characterized the area surface of the nearest green space.

We included air pollutants that were previously found to be associated with white matter microstructure in the Generation R Study: nitrogen oxides (NOx), particulate matter with aerodynamic diameter less than 2.5 μm (PM2.5), silicon in PM2.5, zinc in PM2.5, and oxidative potential of PM2.5 measured by dithiothreitol (OPdtt) (Lubczyńska et al. 2020). Briefly, three two-week measurements of NOx were performed in summer, winter, and intermediate season between February 2009 and February 2010 at 80 sites spread across the Netherlands and Belgium (Beelen et al. 2013). Additionally, PM2.5 levels were measured at 40 of these sites (Eeftens et al. 2012). PM2.5 filters were used to measure the composition of PM2.5 (i.e., silicon and zinc) (de Hoogh et al. 2013) and the oxidative potential of PM2.5 (i.e., OPddt) (Yang et al. 2015). We corrected each measurement for temporal variability of sources, by calculating the difference between the concentration for a specific sampling period and the annual average at a continuous reference monitoring site at a regional background location, and then subtracting that difference from each measurement. We averaged the results of all measurements to obtain one annual mean. Next, we used land use regression models based on a variety of potential land use predictors, to estimate air pollution levels at each address that the participants have lived. We considered the number of days that the participants spent living at each address, and weighted the exposure levels accordingly to this number to obtain mean air pollution concentration of each pollutant for each participant for the pregnancy and for the childhood period. As no historical data was available for most of the air pollutants to perform extrapolation matching the exact periods of the study, we assumed that the spatial contrast remained constant over time as demonstrated in previous studies (Eeftens et al. 2011). In the PELAGIE cohort, annual average NO2 and PM2.5 concentrations were estimated from a land-use regression (LUR) model on a 100-m grid

across Western Europe for the year 2010 (de Hoogh et al. 2018). To obtain estimates for the relevant exposure study period, temporal adjustment was conducted using background routine monitoring stations and calculating the ratio of the concentration of the routine monitor of each day of the study period and the annual average during 2010 as the adjustment factor for that day.

For the road-traffic noise, in the Generation R Study, we used existing EU noise maps developed in 2012 for the municipalities of Rotterdam, Maassluis, Rozenburg, Schiedam, and Vlaardingen (Environmental Noise Directive 2002). We used the day-evening-night level noise indicator (Lden). It was the A-weighted average sound level over 24-hours, with a penalty of 10 dB for night time noise and an additional penalty of 5 dB for evening noise due to higher nuisance perception and greater health impacts during those time periods (WHO Regional Office for Europe 2018). For the PELAGIE cohort, road-traffic noise was not included because it was missing for 65% of the participants.

Table S1. Urban environment data sources

Indicators	Generation R Study	PELAGIE cohort
Building density	European Settlement Map 2017	
Street intersection density and facility richness	NAVTEQ (2012) (Navteq)	
Population density	Global Human Settlement Layer	
Public transport (lines and stops)	Open Street Maps	--
Green and blue spaces, land use	UrbanAtlas (2006-2012)	
NDVI	Landsat 4–5 Thematic Mapper (TM), Landsat 7 Enhanced Thematic Mapper Plus (ETM+), and Landsat 8 Operational Land Imager (OLI)/Thermal Infrared Sensor (TIRS)	
NOx	ESCAPE Project (Brunekreef 2008)	ELAPSE Project (de Hoogh et al. 2018)
PM2.5	ESCAPE Project (Brunekreef 2008)	ELAPSE Project (de Hoogh et al. 2018)
Noise	Gemeente Rotterdam	--

NDVI, Normalized Difference Vegetation Index; NOx, nitrogen oxides; PM2.5, particulate matter with an aerodynamic diameter of less than 2.5 μm.

Table S2. Categories of facility density (Navteq)

Categories	Sub-categories
Business	Business facility, and Industrial zone
Community Services	City hall, Civic/Community center, County council, Court house, Embassy, Government office, Place of worship, Police station, and Post office
Educational Institutions	Higher education, Library, and School
Entertainment	Cinema, Nightlife, and Performing arts
Financial Institutions	ATM, and Bank
Hospitals	Hospital, and Medical service
Parks and Recreation	Amusement park, Bowling centre, Campground, Casino, Golf course, Ice skating rink, Marina, Museum, Park/recreation area, Public sport airport, Sports center, and Sports complex
Restaurants	Coffee shop, and Restaurant
Shopping	Bookstore, Clothing store, Convenience store, Customer eletronic store, Department store, Grocery store, Hardware store, Home specialty store, Office supply, Pharmacy, Shopping, Specialty store, and Sporting goods
Transportation Hubs	Airport, Bus station, Commuter rail station, Ferry terminal, Train station, Hotel, Other accommodation, Ski lift, Winery

Table S3. Categories of land use from Urban Atlas

Categories	Sub-categories	Definition
Artificial surfaces	Urban Fabric Urban	areas with dominant residential use or inner-city areas with central business district and residential use
	Industrial, commercial, public, military, private and transport units	Industrial, commercial, public, military and private units or transport units are predominant
	Mine, dump and construction sites	Strong human influence on soil surface, buildings not dominant
	Artificial non-agricultural vegetated areas	Leisure and recreation use dominate
Agricultural areas, semi-natural areas and wetlands	--	Little / no human influence, agriculture, forestry
Forests (natural and plantation)	--	Little / no human influence, agriculture, forestry
Water	--	--

Methods S2. Diffusion Tensor Imaging

In both cohorts, each child underwent a mock scanning session before the actual MRI session (Binter et al. 2019; White et al. 2018).

Sequence parameters

Generation R Study: Diffusion tensor imaging data were collected with 35-direction echo planar imaging sequence (TR = 12.5 ms, TE = 72 ms, field of view = 240 mm x 240 mm, acquisition Matrix = 120 x 120, slice thickness = 2 mm, number of slices = 65, asset acceleration factor = 2, b = 900 s/mm2).

PELAGIE cohort: DWI data were gathered on 60 slices using an interleaved slice acquisition order, slice thickness of 2 mm, no gap, in-plane resolution = 2 mm × 2 mm and in a 256 mm × 256 mm field of view, TR/TE = 11 000/99 ms, flip angle was 90°, pixel bandwidth =1698 Hz/px, using 30 directions and a b-value of 1000 s/mm2.

Image preprocessing

Image preprocessing was performed with the use of the FMRIB Software Library (FSL), version 5.0.9 (Jenkinson et al. 2012) and the Camino diffusion MRI toolkit (Cook et al. 2006) via the Neuroimaging in Python Pipelines and Interfaces package (Nipype, version 0.92, 7). First, we excluded non-brain tissues using the FSL Brain Extraction Tool then rectified for artifacts induced by eddy currents and for translations or rotations that potentially arose due to minor movement of the head during the scanning session using the FSL "eddy_correct" tool. In order to account for rotations applied to the diffusion data, we used the resulting transformation matrices to rotate the diffusion gradient direction table. Next, using the RESTORE approach, we fitted a diffusion tensor at each voxel, followed by the computation of fractional anisotropy (FA) and mean diffusivity (MD).

Probabilistic tractography

Probabilistic tractography was run on each subject's diffusion data using the fully automated FSL plugin AutoPtx (de Groot et al. 2015). First, we estimated the diffusion parameters at each voxel, accounting for two fiber orientations (Behrens et al. 2003, 2007) using the Bayesian Estimation of Diffusion Parameters Obtained using Sampling Techniques (BESTPOSTx) package from FSL. Next, a predefined set of seed and target masks, supplied by the AutoPtx software, were aligned to each subject's diffusion data in native space using a nonlinear registration. Then, we used the FSL probabilistic fiber tracking algorithm, Probtrackx, to identify connectivity distributions for twelve commonly reported fiber bundles:

cingulum bundle, corticospinal tract, inferior longitudinal fasciculus, superior longitudinal fasciculus, uncinate fasciculus (one per hemisphere), forceps minor and forceps major (interhemispheric), based on the predefined seed and target marks. We normalized the connectivity distributions obtained from the fiber tracking process based on the number of successful seed-to-target attempts, and we introduced a threshold to remove voxels that were unlikely to be part of the true distribution. For each twelve white matter tracts, we assessed average FA and MD values, weighted by the connectivity distribution (i.e., voxels with higher probability of being part of the true distribution receiving higher weight).

Image quality assurance

We assessed diffusion image quality using two methods. First, we used the DTIPrep tool (https://www.nitrc.org/projects/dtiprep/) to automatically examine the data for slice wise variation, characteristic of artifact, in each diffusion-weighted volume. Second, we examined sum-of-squares error (SSE) maps from the diffusion tensor calculations for structured signals indicative of artifact. Each SSE map was rated from 0 to 3 (0: "None",1: "Mild", 2: "Moderate", 3: "Severe"). Rating of 3 was denoted by a structured-pattern high signal intensity in the SSE map on one or more slices (not including, for example, the ventricles or non-brain tissue. Examples include substantial ghosting artifacts, entire slices with high signal intensity (indicative of substantial motion). Ratings of 1 or 2 (mild and moderate artifacts, respectively) were rated when data contained no more than three slices with mildly increased structured signal (i.e., not high/strong, not in ventricles/non-brain areas) in the SSE map. We rated SSE maps independently of the automated DTIPrep results (and vice versa), and thus data could be excluded due to failing any of the checks done. Any cases not excluded by the automated DTIPrep tool but still had a "Severe" score from the SSE rating were also excluded from analyses.

We also examined processed tractography data in two ways. First, we examined the accuracy of the nonlinear registration to standard space to ensure seed and target masks for tractography were properly aligned to native space. We checked nonlinear registration by building a four-dimensional nifti file containing all subjects' coregistered FA maps, such that the fourth dimension was subject. We visually inspected images one at a time for major deviations from the template, either in rotations, translations, or over-warping in certain areas (more than ~ 2 voxels of shift from the template). We also inspected proper whole-brain coverage during this step, and some subjects missing substantial portions of the brain (leading to over-warping of the nonlinear registration) were also flagged. Second, we visually

examined each tract to ensure accurate path reconstruction and flag grossly misclassified voxels in the connectivity distribution.

Construction of whole-brain DTI metrics

In order to better capture associations with relatively small effect sizes that spatially are widespread in the brain, we estimated whole-brain FA and MD. We estimated a whole-brain metric of FA and MD from the average of the twelve tracts FA and MD values, respectively.

Table S4. Distribution between participants and non-participants characteristics

	Generation R Study (N=9610)			PELAGIE cohort (N=3322)		
	Participants (N=2725)	Non-participants (N= 6885)	p.value	Participants (N=95)	Non-participants (N=3227)	p.value
Maternal educational level			<0.001			0.001
primary or lower	6.5	13.3		7.4	19.2	
secondary	39.8	48.6		12.8	19.0	
higher	53.6	38.1		79.8	61.8	
Paternal educational level			<0.001			
primary or lower	5.0	9.9		--	--	
secondary	37.5	42.9		--	--	
higher	57.6	47.2		--	--	
Monthly household income at enrollment			<0.001			
<900€	7.6	14.9		--	--	
900-1,600€	14.0	20.3		--	--	
1,600-2,200€	14.0	15.4		--	--	
>2,200€	64.5	49.4		--	--	
Maternal national origin			<0.001			0.36
The Netherlands	58.7	46.3		--	--	
other Western	8.6	8.6		--	--	
non-Western	32.7	45.2		--	--	
Europe	--	--		100	98.3	
other	--	--		0	1.7	

Table S4. Continuation

	Generation R Study (N=9610)			PELAGIE cohort (N=3322)		
	Participants (N=2725)	Non-participants (N= 6885)	p.value	Participants (N=95)	Non-participants (N=3227)	p.value
Paternal national origin			<0.001			--
The Netherlands	69.4	57.8		--	--	
other Western	6.0	7.2		--	--	
non-Western	24.6	35.0		--	--	
Family status at enrollment			<0.001			0.21
married	52.0	48.9		100	97.4	
living together	36.9	35.2				
no partner	11.0	15.9		0	2.6	
Maternal parity			0.01			0.02
no child	55.8	55.0		32.6	44.9	
≥ 1 child	44.2	45.0		67.4	55.1	
Maternal smoking during pregnancy			<0.001			<0.001
never	78.4	71.5		100	84.8	
until pregnancy known	8.3	8.6				
during pregnancy	13.3	19.9		0	15.2	

Table S4. Continuation

	Generation R Study (N=9610)			PELAGIE cohort (N=3322)		
	Participants (N=2725)	Non-participants (N= 6885)	p.value	Participants (N=95)	Non-participants (N=3227)	p.value
Maternal alcohol use during pregnancy			<0.001			0.02
never	49.2	53.0		100	70.9	
				0	14.9	
until pregnancy known	--	13.4				
during pregnancy	--	33.6		0	14.4	
<1 drink per week	28.6			--	--	
1-6 drinks per week	19.1			--	--	
≥1 drink per day	3.1			--	--	
Paternal age at enrollment (years)	33.6 ± 5.3	32.4 ± 5.9	<0.001	--	--	--
Maternal pre-pregnancy BMI (kg/cm2)	23.5 ± 4	23.7 ± 4.5	0.002	22.0 ± 3.3	22.5 ± 4.1	0.17
Paternal BMI (kg/cm2)	25.2 ± 3.3	25.3 ± 3.6	0.13	--	--	--
Maternal height (cm)	168.1 ± 7.4	166.7 ± 7.4	<0.001	165.6 ± 6.6	164.0 ± 5.8	0.03
Paternal height (cm)	182.6 ± 7.7	181.2 ± 8.0	<0.001	--	--	--
Maternal psychological distress during pregnancy	0.3 ± 0.3	0.3 ± 0.4	<0.001	--	--	--
Paternal psychological distress during pregnancy	0.1 ± 0.2	0.2 ± 0.3	<0.001	--	--	--
Maternal IQ score	98.0 ± 14.6	94.2 ± 15.7	<0.001	94.5 ± 10.5	92.7 ± 11.7	0.23
Child's sex			0.308			0.13
boy	50.0	50.9		42.1	50.5	
girl	50.0	49.1		57.9	49.5	

Values are mean±standard deviation for continuous variables and percentage for categorical variables.

Figure S1. Directed acyclic graphs

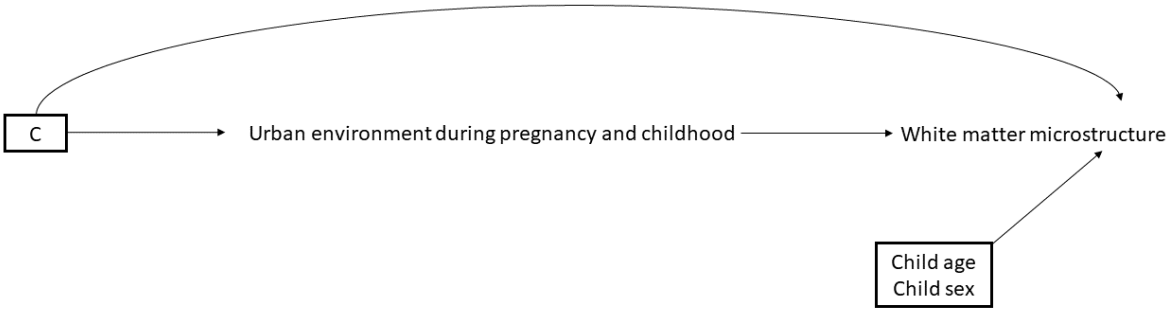

C denotes all the potential confounding variables in the relationship between urban environment during pregnancy and childhood and white matter microstructure in preadolescence, such as socioeconomic status, parental lifestyle and ethnicity.
In our study we included: for maternal and paternal educational levels, monthly household income, maternal and paternal national origin, maternal and paternal age at enrollment in the cohort, maternal smoking and alcohol use during pregnancy, parity, marital status, maternal and paternal psychological distress, maternal and paternal BMI and height, maternal intelligence quotient, child's sex and age at the MRI session.
The ***box*** indicates the conditioning on the potential confounders. ***Arrows*** represent existing pathways indicating thereby the direction of the associations.

Methods S3. Multiple imputation of potential confounders

Missing values of potential confounders were imputed using the method of chained equations, using the *mice* package in R. Covariates were used as predictor of a given variable if they were correlated with the levels and/or the probability of the given variable being missing (absolute correlation value >0.3). We also ensured that for each predictor, the proportion of observed values was greater than 50%. After imputation, we conducted the following diagnostics. We compared imputed and observed data using density plots and stripplots of van Buuren and Greenacre (van Buuren and Greenacre 2018). These types of comparison were only done when there were more than 5% of non-observed values. Numerically, we checked that variables had i) an absolute difference between means of the observed and imputed values smaller than 2 standard deviations; and ii) a ratio of variances of the observed and imputed values between 0.5 and 2. For categorical variables, we ensured the p-value of the chi-squared test between imputed and non-imputed values was >0.05.

Methods S4. Inverse probability weighting

We applied inverse probability weighting to correct for potential attrition bias. We used covariates of all eligible liveborn singletons (N=9,610 in the Generation R Study and N= 3,322 in the PELAGIE cohort) to predict the probability of participation (N=2,725 in the Generation R Study and N=95 in the PELAGIE cohort), and we applied the inverse of those probabilities as weights in all the regression analyses. In the Generation R Study, families of the included participants were more likely to have higher education, have higher household income, be Dutch, and to be married, as compared to families of participants not included (Table S5). In the PELAGIE cohort, mothers of the participants were more likely to have higher education.

Generation R Study

For calculation of the weights in the Generation R Study , we considered parental age, participation of the partner in the study, national origin, child's national origin, parental education, marital status, household income, intake period (prenatal vs. postnatal), parity, maternal weight, parental body mass index, maternal height, maternal smoking during pregnancy, maternal alcohol consumption during pregnancy, gestational birth weight, parental psychological distress, maternal intelligence quotient, child's gender, and child's genetic ancestry. The variables selected ($p<0.25$) were maternal age, participation of the partner in the study, national origin, maternal education, household income, intake period, parity, maternal weight, maternal body mass index, maternal height, gestational birth weight, maternal smoking during pregnancy, maternal intelligence quotient, and child's genetic ancestry. Then, to reduce the influence of extreme values, we used the most significant variables ($p<0.01$), i.e. maternal age, participation of the partner in the study, household income, intake period, parity, gestational birth weight, maternal smoking during pregnancy, and maternal IQ, to calculate the final weights.

PELAGIE cohort

For calculation of the weights in the PELAGIE cohort, we considered maternal age, education, socioeconomic category, parity, second-hand smoke exposure during pregnancy, body mass index, height, gestational age at birth, and child's gender. The variables selected ($p<0.25$) were maternal education, socioeconomic category, parity, height, second-hand smoke, and

child's gender. Then, to reduce the influence of extreme values, we used the most significant variables ($p<0.01$), i.e. maternal education and parity, to calculate the final weights.

Figure S2. Schematic figure of the statistical analyses

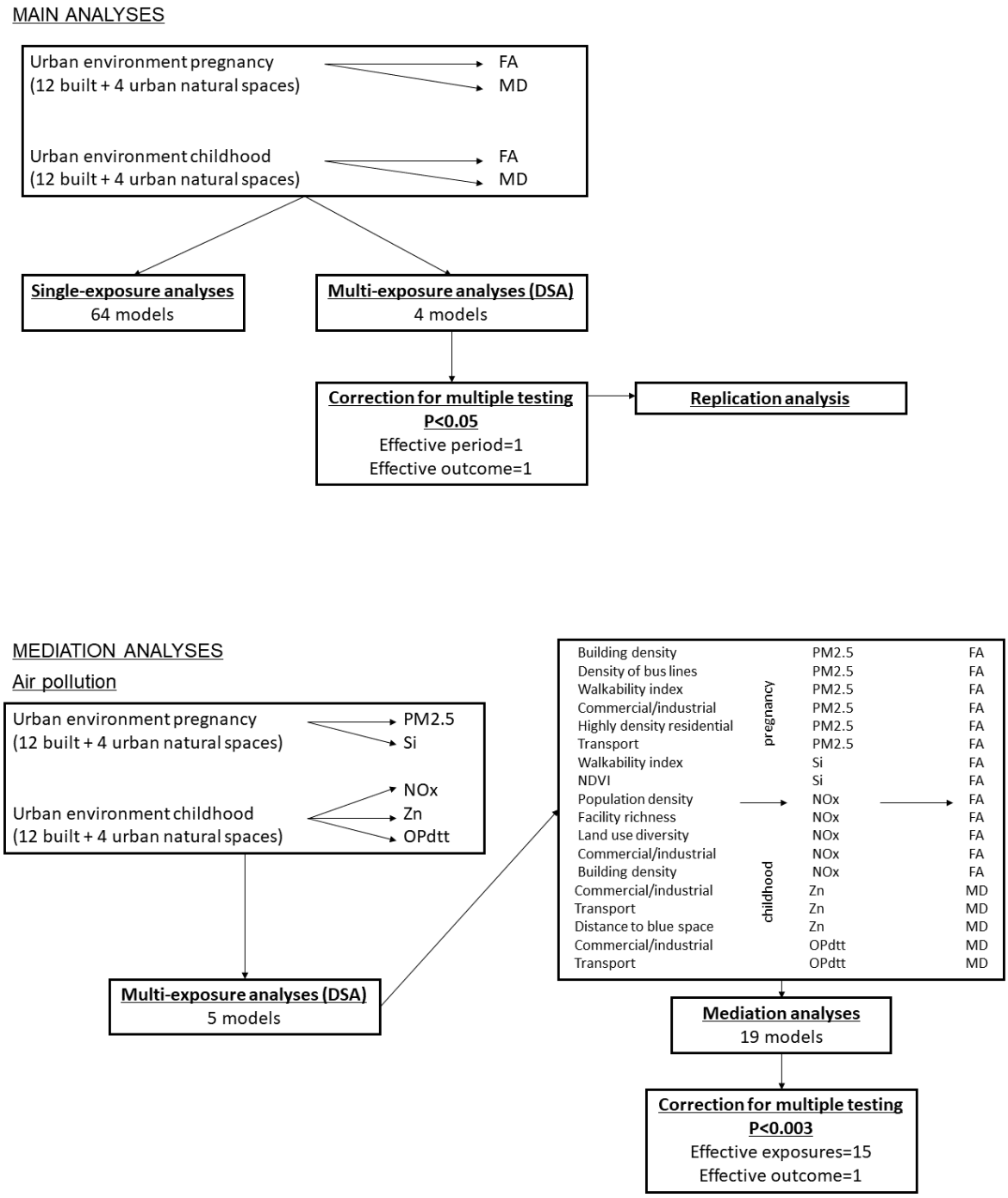

MEDIATION ANALYSES

Road-traffic noise

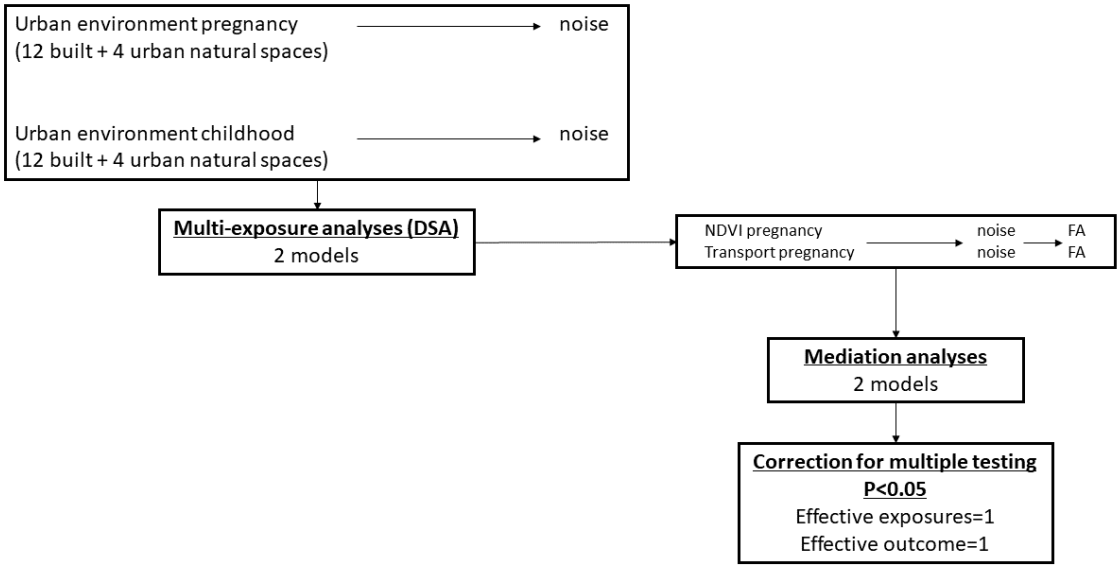

Methods S5. Deletion-substitution-addition algorithm

The Deletion-Substitution-Addition algorithm is an iterative selection method, which selects the variables that are most predictive of the outcome by cross-validation, taking into account the correlation matrix of the variables. At each iteration, the algorithm allows three steps, namely: i) deletion, removal of a variable; ii) substitution, replacement of one variable with another; and iii) addition, insertion of a variable to the model. The process to the optimal model (i.e. a combination of variables with the smallest value of root-mean-square deviation) starts with a model containing only the intercept, and continues with the deletion, substitution, and addition processes. To assure the adjustment for all potential confounding variables in each model, we fixed the potential confounding variables (including the area), allowing only the exposure variables to participate in the selection process.

Methods S6. Equations of the single-exposure and mediation models

A-Single-exposure models

$$E[Y|a,c] = \beta_o + \beta_1 a + \beta_2 c$$

Y denotes the outcomes (i.e., whole-brain fractional anisotropy and mean diffusivity), **a** denotes all the selected exposures (i.e., built environment and urban natural spaces), **m** denotes all the potential mediators (i.e., air pollutants and traffic-related noise), and **c** denotes all the potential confounders (i.e., parental educational levels, monthly household income, parental national origin, parental age at enrollment in the cohort, maternal smoking and alcohol use during pregnancy, parity, marital status, parental psychological distress, parental BMI and height, maternal intelligence quotient, child's sex and age at the MRI session). We assumed that there is not exposure-mediation in our analyses (i.e., θ_3 being null).

B-Mediation models (Valeri and VanderWeele 2013)

$$E[Y|a,m,c] = \theta_o + \theta_1 a + \theta_2 m + \theta_3 c$$

Y denotes the outcomes (i.e., whole-brain fractional anisotropy and mean diffusivity), **a** denotes all the selected exposures (i.e., built environment and urban natural spaces), **m** denotes all the selected mediators (i.e., air pollutants and traffic-related noise), and **c** denotes all the potential confounders (i.e., parental educational levels, monthly household income, parental national origin, parental age at enrollment in the cohort, maternal smoking and alcohol use during pregnancy, parity, marital status, parental psychological distress, parental BMI and height, maternal intelligence quotient, child's sex and age at the MRI session).

Figure S3. Correlations between exposures in the Generation R Study

Pregnancy period

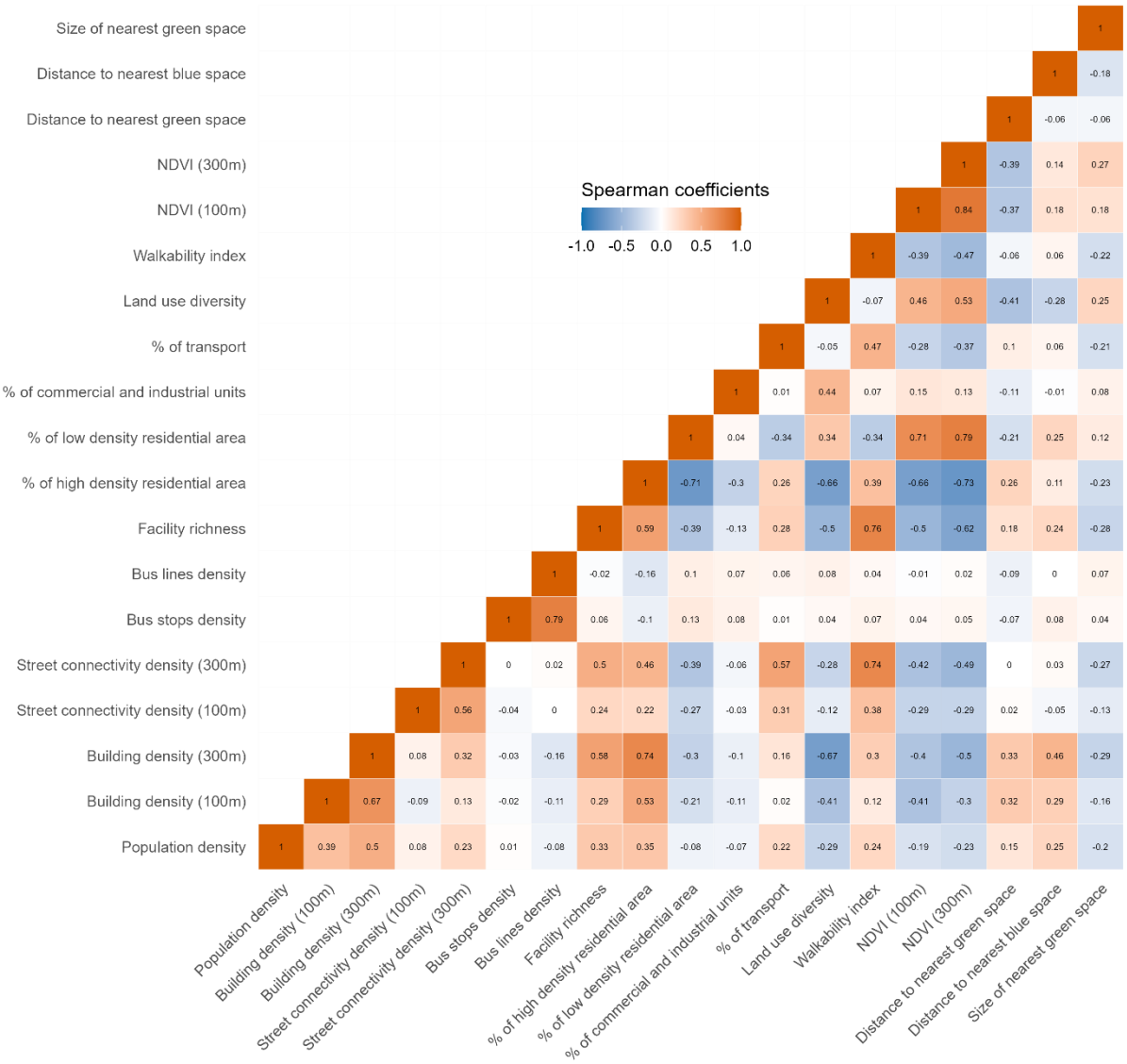

Childhood period

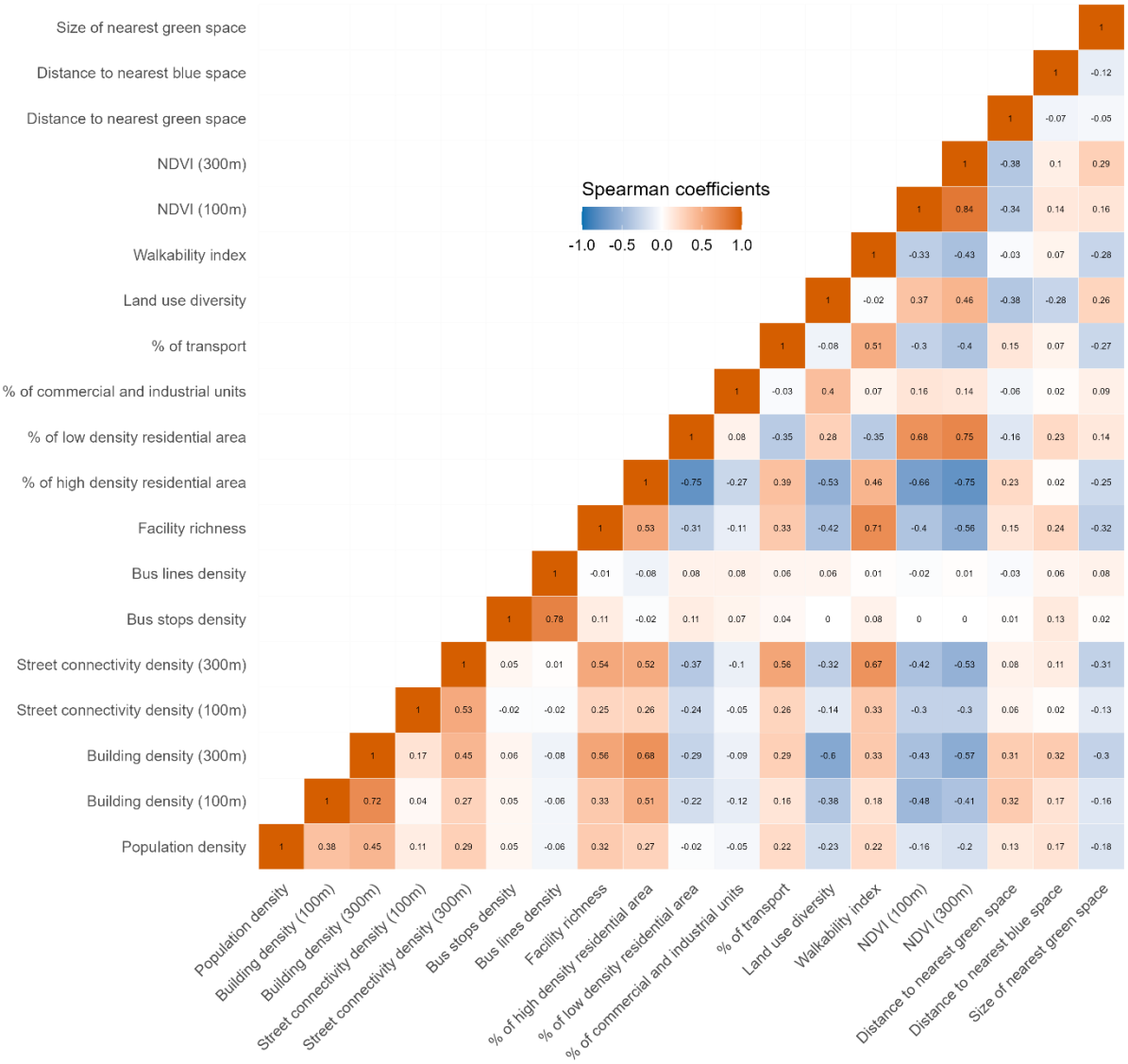

NDVI, Normalized Difference Vegetation Index.

Table S5. Distribution of the white matter microstructure metrics in the Generation R Study (N=2,725)

							Correlations	
Metric	mean ± sd	min	p25	p50	p75	max	with FA	with MD
Whole-brain FA	0.457 ± 0.017	0.356	0.446	0.457	0.468	0.513	1.00	-0.55
left cingulum bundle FA	0.419 ± 0.044	0.236	0.390	0.421	0.449	0.604	0.65	-0.24
right cingulum bundle FA	0.374 ± 0.040	0.233	0.348	0.374	0.401	0.512	0.59	-0.22
left corticospinal tract FA	0.542 ± 0.021	0.411	0.528	0.542	0.556	0.613	0.53	-0.27
right corticospinal tract FA	0.53 ± 0.021	0.413	0.517	0.531	0.544	0.602	0.53	-0.28
left inferior longitudinal fasciculus FA	0.428 ± 0.022	0.309	0.414	0.428	0.443	0.502	0.57	-0.45
right inferior longitudinal fasciculus FA	0.438 ± 0.022	0.346	0.423	0.438	0.453	0.515	0.60	-0.44
left superior longitudinal fasciculus FA	0.397 ± 0.022	0.320	0.383	0.397	0.411	0.471	0.64	-0.42
right superior longitudinal fasciculus FA	0.396 ± 0.024	0.296	0.380	0.396	0.412	0.473	0.67	-0.42
left uncinate fasciculus FA	0.388 ± 0.030	0.269	0.369	0.389	0.408	0.486	0.56	-0.23
right uncinate fasciculus FA	0.396 ± 0.027	0.217	0.378	0.397	0.414	0.504	0.64	-0.29
forceps minor FA	0.604 ± 0.032	0.449	0.583	0.604	0.624	0.716	0.57	-0.32
forceps major FA	0.572 ± 0.034	0.302	0.552	0.574	0.595	0.708	0.48	-0.51

Table S5. Continuation

							Correlations	
Metric	mean ± sd	min	p25	p50	p75	max	with FA	with MD
Whole-brain MD	0.809 ± 0.021	0.667	0.796	0.808	0.822	1.046	-0.55	1.00
left cingulum bundle MD	0.789 ± 0.029	0.702	0.769	0.789	0.808	0.913	-0.39	0.68
right cingulum bundle MD	0.798 ± 0.028	0.715	0.779	0.798	0.817	0.908	-0.37	0.68
left corticospinal tract MD	0.774 ± 0.045	0.623	0.761	0.772	0.784	2.678	-0.39	0.65
right corticospinal tract MD	0.782 ± 0.045	0.567	0.769	0.780	0.792	2.901	-0.39	0.65
left inferior longitudinal fasciculus MD	0.836 ± 0.028	0.760	0.819	0.833	0.851	1.274	-0.46	0.81
right inferior longitudinal fasciculus MD	0.836 ± 0.032	0.734	0.814	0.833	0.854	1.028	-0.41	0.74
left superior longitudinal fasciculus MD	0.782 ± 0.023	0.715	0.766	0.779	0.796	0.881	-0.52	0.81
right superior longitudinal fasciculus MD	0.774 ± 0.026	0.696	0.757	0.773	0.791	0.904	-0.54	0.77
left uncinate fasciculus MD	0.819 ± 0.022	0.744	0.805	0.819	0.833	1.137	-0.46	0.65
right uncinate fasciculus MD	0.825 ± 0.022	0.644	0.811	0.824	0.839	0.945	-0.41	0.66
forceps minor MD	0.826 ± 0.031	0.707	0.805	0.824	0.845	1.000	-0.37	0.64
forceps major MD	0.872 ± 0.066	0.654	0.826	0.864	0.907	1.263	-0.21	0.55

FA: fractional anisotropy; MD: mean diffusivity; mean ± sd: mean and standard deviation; min: minimal value; max: maximal value; p25-p50-p75: percentile 25-percentile 50-percentile 75. Correlations based on Spearman coefficients.

Table S6. Distribution of the white matter microstructure metrics in the PELAGIE cohort (N=95)

							Correlations	
Metric	mean ± sd	min	p25	p50	p75	max	with FA	with MD
Whole-brain FA	0.519 ± 0.017	0.475	0.506	0.52	0.529	0.574	1	-0.71
left cingulum bundle FA	0.532 ± 0.039	0.436	0.506	0.527	0.56	0.616	0.66	-0.32
right cingulum bundle FA	0.476 ± 0.04	0.362	0.45	0.471	0.508	0.551	0.61	-0.35
left corticospinal tract FA	0.559 ± 0.024	0.516	0.539	0.559	0.573	0.619	0.66	-0.44
right corticospinal tract FA	0.557 ± 0.023	0.506	0.54	0.558	0.572	0.618	0.63	-0.44
left inferior longitudinal fasciculus FA	0.509 ± 0.023	0.452	0.495	0.508	0.524	0.561	0.4	-0.36
right inferior longitudinal fasciculus FA	0.519 ± 0.023	0.446	0.504	0.521	0.534	0.584	0.58	-0.48
left superior longitudinal fasciculus FA	0.447 ± 0.022	0.386	0.432	0.447	0.462	0.502	0.7	-0.64
right superior longitudinal fasciculus FA	0.437 ± 0.02	0.382	0.427	0.438	0.448	0.485	0.62	-0.58
left uncinate fasciculus FA	0.463 ± 0.028	0.401	0.445	0.46	0.485	0.564	0.61	-0.5
right uncinate fasciculus FA	0.461 ± 0.025	0.391	0.448	0.462	0.48	0.513	0.57	-0.47
forceps minor FA	0.65 ± 0.027	0.58	0.633	0.649	0.667	0.739	0.66	-0.37
forceps major FA	0.616 ± 0.027	0.535	0.601	0.615	0.634	0.682	0.5	-0.35

Table S6. Continuation

							Correlations	
Metric	mean ± sd	min	p25	p50	p75	max	with FA	with MD
Whole-brain MD	0.805 ± 0.018	0.753	0.794	0.805	0.818	0.842	-0.71	1
left cingulum bundle MD	0.775 ± 0.023	0.728	0.76	0.772	0.79	0.833	-0.36	0.63
right cingulum bundle MD	0.796 ± 0.025	0.732	0.778	0.798	0.812	0.861	-0.54	0.71
left corticospinal tract MD	0.765 ± 0.028	0.695	0.747	0.763	0.782	0.86	-0.57	0.62
right corticospinal tract MD	0.763 ± 0.028	0.697	0.744	0.761	0.776	0.832	-0.52	0.57
left inferior longitudinal fasciculus MD	0.832 ± 0.023	0.763	0.816	0.833	0.848	0.886	-0.46	0.75
right inferior longitudinal fasciculus MD	0.834 ± 0.023	0.77	0.82	0.834	0.849	0.884	-0.56	0.75
left superior longitudinal fasciculus MD	0.786 ± 0.024	0.724	0.772	0.786	0.802	0.862	-0.48	0.73
right superior longitudinal fasciculus MD	0.788 ± 0.024	0.725	0.773	0.785	0.8	0.876	-0.56	0.81
left uncinate fasciculus MD	0.832 ± 0.028	0.754	0.817	0.832	0.848	0.898	-0.57	0.78
right uncinate fasciculus MD	0.837 ± 0.023	0.772	0.82	0.839	0.849	0.903	-0.55	0.72
forceps minor MD	0.773 ± 0.026	0.702	0.758	0.774	0.794	0.826	-0.43	0.64
forceps major MD	0.881 ± 0.049	0.769	0.852	0.883	0.909	1	-0.26	0.42

FA: fractional anisotropy; MD: mean diffusivity; mean ± sd: mean and standard deviation; min: minimal value; max: maximal value; p25-p50-p75: percentile 25-percentile 50-percentile 75. Correlations based on Spearman coefficients.

Table S7. Single-exposure association between urban environment indicators and whole-brain fractional anisotropy in the Generation R Study

	Pregnancy period		Childhood period	
	Δ	Estimate (95%CI)	Δ	Estimate (95%CI)
Population density (inhabitants/km²)	206	0.000048 (-0.00015; 0.00025)	768	-0.000388 (-0.00093; 0.00015)
Building density (km²/km²)	157895	0.000701 (-0.00021; 0.00161)	150335	-0.000013 (-0.00095; 0.00092)
Street intersection density (intersections/km²)	4.11	-0.000004 (-0.00094; 0.00093)		-0.000254 (-0.00118; 0.00067)
Density of bus stops (stops/km², 300-m buffer)	0.54	-0.000338 (-0.00172; 0.00105)	0.33	-0.000904 (-0.00187; 6e-05)
Density of bus lines (m/km², 300-m buffer)	5.29	0.000693 (-0.00069; 0.00207)	2.56	-0.000185 (-0.00097; 6e-04)
Facility richness (facility types/km², 300-m buffer)	0.007	0.000196 (-0.00081; 0.0012)	0.006	-0.00015 (-0.00119; 0.00089)
Land use diversity (300-m buffer)	0.14	-0.000718 (-0.00161; 0.00018)	0.12	-0.000095 (-0.00093; 0.00074)
Walkability index (300-m buffer)	0.075	-0.000315 (-0.00112; 0.00049)	0.072	-0.000511 (-0.00143; 0.00041)
% of high density residential land use	2.92	0.000403 (-0.00049; 0.00129)	3.18	0.000057 (-0.00097; 0.00108)
% of low density residential land use	26.8	-0.00033 (-0.0013; 0.00064)	30.7	-0.000574 (-0.0015; 0.00035)
% of commercial and industrial units	0.34	-0.000003 (-0.00087; 0.00087)	0.30	0.00022 (-0.0008; 0.00124)
% of transport	7.35	0.000129 (-0.00068; 0.00093)	6.71	-0.000167 (-0.00097; 0.00064)
NDVI	0.14	-0.000677 (-0.00163; 0.00028)	0.13	0.000153 (-0.00086; 0.00117)
Distance to nearest major green space (m)	7.0	0.000969 (0.0001; 0.00184)	6.2	0.000643 (-0.00022; 0.0015)
Distance to nearest major blue space (m)	10.0	0.000195 (-0.00073; 0.00111)	8.6	0.000436 (-0.00041; 0.00128)
Area of the nearest major green space (m^2)	0.004	-0.000243 (-0.00116; 0.00068)	0.004	0.000436 (-0.00041; 0.00128)

Adjusted for maternal and paternal educational levels, monthly household income, maternal and paternal national origin, maternal and paternal age at enrollment in the cohort, maternal smoking and alcohol use during pregnancy, parity, marital status, maternal and paternal psychological distress, maternal and paternal BMI and height, maternal intelligence quotient, child's sex and age at the MRI session.

NDVI, Normalized Difference Vegetation Index.

Table S8. Single-exposure association between urban environment indicators and whole-brain mean diffusivity in the Generation R Study

	Pregnancy period		Childhood period	
	Δ	Estimate (95%CI)	Δ	Estimate (95%CI)
Population density (inhabitants/km²)	206	-0.00038 (-0.00028; 0.0002)	768	0.00042 (-0.00061; 0.00069)
Building density (km²/km²)	157895	0.000535 (-0.00056; 0.00163)	150335	0.000572 (-0.00055; 0.0017)
Street intersection density (intersections/km²)	4.11	0.00085 (-0.00027; 0.00197)	3.41	0.000657 (-0.00046; 0.00177)
Density of bus stops (stops/km², 300-m buffer)	0.54	-0.000319 (-0.00199; 0.00135)	0.33	0.000203 (-0.00096; 0.00136)
Density of bus lines (m/km², 300-m buffer)	5.29	-0.001408 (-0.00307; 0.00025)	2.56	-0.000116 (-0.00106; 0.00082)
Facility richness (facility types/km², 300-m buffer)	0.007	0.000922 (-0.00028; 0.00213)	0.006	0.001129 (-0.00012; 0.00238)
Land use diversity (300-m buffer)	0.14	-0.000657 (-0.00173; 0.00042)	0.12	-0.001201 (-0.00221; -0.00019)
Walkability index (300-m buffer)	0.075	0.000746 (-0.00022; 0.00171)	0.072	0.000652 (-0.00046; 0.00176)
% of high density residential land use	2.92	0.000324 (-0.00075; 0.00139)	3.18	0.000365 (-0.00087; 0.0016)
% of low density residential land use	26.8	0.000207 (-0.00096; 0.00137)	30.7	0.0002 (-0.00091; 0.00131)
% of commercial and industrial units	0.34	-0.000058 (-0.0011; 0.00099)	0.30	-0.000301 (-0.00153; 0.00093)
% of transport	7.35	0.000006 (-0.00096; 0.00097)	6.71	0.00025 (-0.00072; 0.00122)
NDVI	0.14	-0.000233 (-0.00138; 0.00091)	0.13	-0.000572 (-0.00179; 0.00065)
Distance to nearest major green space (m)	7.0	-0.000409 (-0.00145; 0.00063)	6.2	-0.000436 (-0.00147; 0.0006)
Distance to nearest major blue space (m)	10.0	-0.000019 (-0.00112; 0.00109)	8.6	0.000382 (-0.00063; 0.0014)
Area of the nearest major green space (m^2)	0.004	0.000643 (-0.00047; 0.00175)	0.004	0.000382 (-0.00063; 0.0014)

Adjusted for maternal and paternal educational levels, monthly household income, maternal and paternal national origin, maternal and paternal age at enrollment in the cohort, maternal smoking and alcohol use during pregnancy, parity, marital status, maternal and paternal psychological distress, maternal and paternal BMI and height, maternal intelligence quotient, child's sex and age at the MRI session.

NDVI, Normalized Difference Vegetation Index.

Table S9. Associations between urban environment indicators and white matter microstructure in the Generation R Study with minimal set of adjustment

	Δ	Pregnancy period	Childhood period
		Estimate (95%CI)	Estimate (95%CI)
Whole-brain fractional anisotropy			
distance to the nearest major green space	7m	0.00091 (0.00005; 0.0018)	
Whole-brain mean diffusivity			
land use diversity	0.12		-0.001 (-0.002; -0.0003)

Adjusted for maternal educational level, age at enrollment in the cohort, parity, height, body mass index, intelligence quotient, child's sex and age at the magnetic resonance imaging session.

CI: Confidence interval.

Table S10. Replication of the associations between urban environment indicators and white matter microstructure in the PELAGIE cohort

	Δ	Pregnancy period	Childhood period
		Estimate (95%CI)	Estimate (95%CI)
Whole-brain fractional anisotropy			
distance to the nearest major green space	7m	0.000002 (-0.000002; 0.00005)	
Whole-brain mean diffusivity			
land use diversity	0.12		-0.006 (-0.02; 0.01)

Adjusted for maternal educational level, age at enrollment in the cohort, parity, height, body mass index, intelligence quotient, child's sex and age at the magnetic resonance imaging session.

CI: Confidence interval.

Table S11. Associations between built environment and urban natural spaces indicators, and air pollution and road-traffic noise in the Generation R Study (N=2,725)

	Unit of increase in exposure	Estimate (95%CI)
Prenatal levels of PM2.5		
building density [b]	0.00018	-0.14 (-0.18; -0.10)
density of bus lines [a]	5.30	-0.13 (-0.18; -0.09)
walkability index	0.08	0.10 (0.07; 0.11)
% of commercial and industrial units [a]	0.34	0.14 (0.11; 0.18)
% of high density residential area [b]	2.92	0.11 (0.06; 0.15)
% of transport	7.35	0.18 (0.15; 0.21)
Prenatal concentrations of silicon in PM2.5		
walkability index	0.08	2.06 (1.26; 2.87)
NDVI	0.1	-1.73 (-2.69; -0.78)
Childhood levels of NOx		
population density	7.68	1.26 (0.85; 1.67)
facility richness [a]	0.01	2.67 (1.80; 3.55)
land use diversity	0.12	2.42 (1.71; 3.15)
% of commercial and industrial units [a]	0.30	2.53 (1.81; 3.25)
% of transport	6.71	5.13 (4.51; 5.74)
Childhood concentrations of zinc in PM2.5		
building density [b]	0.16	-1.13 (-1.37; -0.89)
% of commercial and industrial units [a]	0.30	0.67 (0.45; 0.89)
% of transport	6.71	2.11 (1.92; 2.32)
distance to the nearest major blue space [b]	8.56	0.58 (0.37; 0.80)

Table S11. Continuation

	Unit of increase in exposure	Estimate (95%CI)
Childhood levels of OPdtt		
% of commercial and industrial units [a]	0.30	0.49 (0.04; 0.94)
% of transport	6.71	1.68 (1.30; 2.07)
Prenatal levels of road-traffic noise		
% of transports	6.71	1.74 (1.33; 2.15)
NDVI	0.1	-1.42 (-1.90; -0.94)

A: log-transformed, b: squared-transformed.

Adjusted for parental educational levels, monthly household income, parental national origin, parental age at enrollment in the cohort, maternal smoking and alcohol use during pregnancy, parity, marital status, parental psychological distress, parental body mass index and height, maternal intelligence quotient, child's sex and age at the magnetic resonance imaging session.

CI: Confidence interval; NOx: nitrogen oxides; PM2.5: particulate matter with aerodynamic diameter less than 2.5 μm; OPdtt: oxidative potential of PM2.5 measured by dithiothreitol.

Table S12. Associations between noise exposure and white matter microstructure in the Generation R Study

		FA	MD
	Unit of increase in exposure	Coef. (95%CI)	Coef. (95%CI)
Pregnancy period	10 dB	-0.001 (-0.002; -0.000)	-0.0004 (-0.001; 0.0005)
Childhood period	10 dB	0.0005 (-0.001; 0.001)	0.0003 (-0.001; 0.001)

FA: fractional anisotropy; MD: mean diffusivity.

Adjusted for parental educational levels, monthly household income, parental national origin, parental age at enrollment in the cohort, maternal smoking and alcohol use during pregnancy, parity, marital status, parental psychological distress, parental BMI and height, maternal intelligence quotient, child's sex and age at the MRI session.

Figure S4. Types of urban green spaces in the Generation R Study

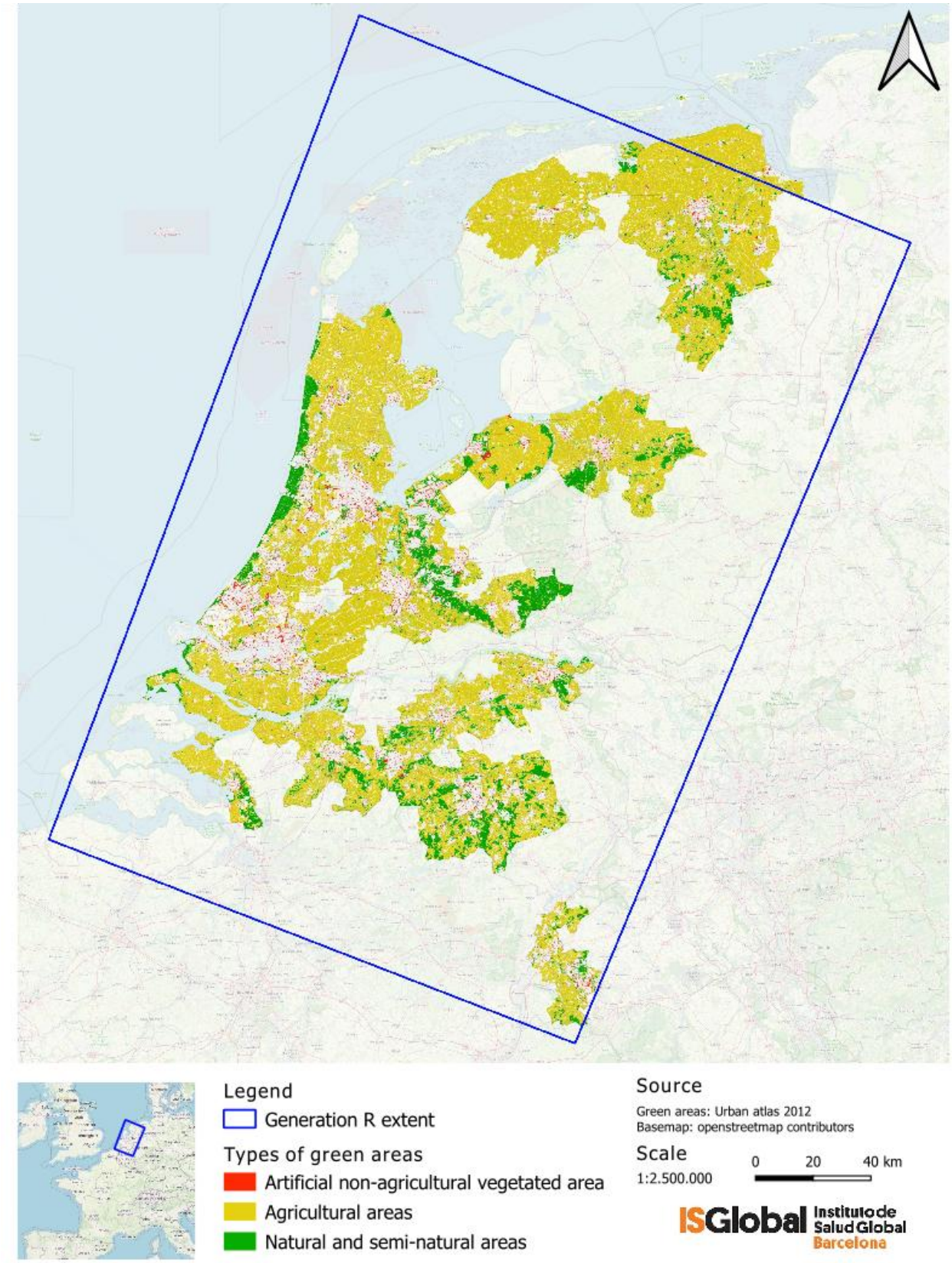

Generation R participants mostly reside in the Rotterdam and surrounding urban areas.

References

Beelen R, Hoek G, Vienneau D, Eeftens M, Dimakopoulou K, Pedeli X, et al. 2013. Development of NO2 and NOx land use regression models for estimating air pollution exposure in 36 study areas in Europe – The ESCAPE project. Atmospheric Environment 72:10–23; doi:10.1016/j.atmosenv.2013.02.037.

Behrens TEJ, Berg HJ, Jbabdi S, Rushworth MFS, Woolrich MW. 2007. Probabilistic diffusion tractography with multiple fibre orientations: What can we gain? NeuroImage 34:144–155; doi:10.1016/j.neuroimage.2006.09.018.

Behrens TEJ, Woolrich MW, Jenkinson M, Johansen-Berg H, Nunes RG, Clare S, et al. 2003. Characterization and propagation of uncertainty in diffusion-weighted MR imaging. Magnetic Resonance in Medicine 50:1077–1088; doi:10.1002/mrm.10609.

Binter A-C, Bannier E, Simon G, Saint-Amour D, Ferré J-C, Barillot C, et al. 2019. Prenatal exposure to glycol ethers and motor inhibition function evaluated by functional MRI at the age of 10 to 12 years in the PELAGIE mother-child cohort. Environment International 133:105163; doi:10.1016/j.envint.2019.105163.

Brunekreef B. 2008. ESCAPE Study Manual.

Cook PA, Bai Y, Nedjati-Gilani S, Seunarine KK, Hall MG, Parker GJ, et al. 2006. Camino: Open-Source Diffusion-MRI Reconstruction and Processing. 1.

de Groot M, Ikram MA, Akoudad S, Krestin GP, Hofman A, van der Lugt A, et al. 2015. Tract-specific white matter degeneration in aging: The Rotterdam Study. Alzheimer's & Dementia 11:321–330; doi:10.1016/j.jalz.2014.06.011.

de Hoogh K, Chen J, Gulliver J, Hoffmann B, Hertel O, Ketzel M, et al. 2018. Spatial PM2.5, NO2, O3 and BC models for Western Europe - Evaluation of spatiotemporal stability. Environ Int 120:81–92; doi:10.1016/j.envint.2018.07.036.

de Hoogh K, Wang M, Adam M, Badaloni C, Beelen R, Birk M, et al. 2013. Development of Land Use Regression Models for Particle Composition in Twenty Study Areas in Europe. Environ Sci Technol 47:5778–5786; doi:10.1021/es400156t.

Eeftens M, Beelen R, de Hoogh K, Bellander T, Cesaroni G, Cirach M, et al. 2012. Development of Land Use Regression Models for PM2.5, PM2.5 Absorbance, PM10 and PMcoarse in 20 European Study Areas; Results of the ESCAPE Project. Environ Sci Technol 46:11195–11205; doi:10.1021/es301948k.

Eeftens M, Beelen R, Fischer P, Brunekreef B, Meliefste K, Hoek G. 2011. Stability of measured and modelled spatial contrasts in NO(2) over time. Occup Environ Med 68:765–770; doi:10.1136/oem.2010.061135.

Environmental Noise Directive. 2002. Directive 2002/49/EC. Available: https://environment.ec.europa.eu/topics/noise/environmental-noise-directive_en [accessed 24 May 2023].

Frank LD, Sallis JF, Conway TL, Chapman JE, Saelens BE, Bachman W. 2006. Many Pathways from Land Use to Health: Associations between Neighborhood Walkability and Active Transportation, Body Mass Index, and Air Quality. Journal of the American Planning Association 72:75–87; doi:10.1080/01944360608976725.

Jenkinson M, Beckmann CF, Behrens TEJ, Woolrich MW, Smith SM. 2012. FSL. Neuroimage 62:782–790; doi:10.1016/j.neuroimage.2011.09.015.

Lubczyńska MJ, Muetzel RL, El Marroun H, Basagaña X, Strak M, Denault W, et al. 2020. Exposure to Air Pollution during Pregnancy and Childhood, and White Matter Microstructure in Preadolescents. Environmental Health Perspectives 128:027005; doi:10.1289/EHP4709.

Navteq. Available: https://www.here.com/navteq [accessed 15 February 2023].

Valeri L, VanderWeele TJ. 2013. Mediation analysis allowing for exposure–mediator interactions and causal interpretation: Theoretical assumptions and implementation with SAS and SPSS macros. Psychological Methods 18:137–150; doi:10.1037/a0031034.

van Buuren S, Greenacre M. 2018. *Flexible Imputation of Missing Data*. Second. New York.

White T, Muetzel RL, El Marroun H, Blanken LME, Jansen P, Bolhuis K, et al. 2018. Paediatric population neuroimaging and the Generation R Study: the second wave. Eur J Epidemiol 33:99–125; doi:10.1007/s10654-017-0319-y.

WHO Regional Office for Europe. 2018. Noise guidelines.

Yang A, Wang M, Eeftens M, Beelen R, Dons E, Leseman DLAC, et al. 2015. Spatial Variation and Land Use Regression Modeling of the Oxidative Potential of Fine Particles. Environ Health Perspect 123:1187–1192; doi:10.1289/ehp.1408916.